ChemPubSoc Europe

DOI: 10.1002/chem.201804897

CHEMISTRY A European Journal Communicatio

Axial Coordination

Single-Sided Competitive Axial Coordination of G-Quadruplex/Hemin as Molecular Switch for Imaging Intracellular Nitric Oxide

Lei Zhang[+],[a, b] Jun Zhou[+],[a] Fengjiao Ma[+],[a] Quanbo Wang,[c] Hui Xu,*[b] Huangxian Ju,*[a] and Jianping Lei*[a]

Abstract: Axial coordination is a crucial biological process to regulate biomolecules' functions in natural enzymes. However, it is a great challenge to determine the single or dual axial interaction between the metal center of enzymes and the ligand. In this work, a controllable axial coordination system was developed based on G-quadruplex/hemin complex by designing a series of fluorescent derivatives. The mechanism on axial coordination of G-quadruplex/hemin with coumarin-imidazole ligands was proposed to be single-sided, and led to fluorescence quenching of ligands. Upon addition of nitric oxide, the fluorescence of ligands was recovered through competitive axial coordination, providing a "signal on" strategy for signal transduction. More significantly, the fluorescent imaging of intracellular nitric oxide was achieved after conjugating with gold nanoparticles. Also, the proposed protocol provided a smart strategy to monitor the relationship between nitric oxide and p53 protein activity in living cells.

In natural enzymes, the axial coordination between the active site of metalloenzyme and the small biomolecule ligand plays a significant role in regulating biological functions.[1] Inspirationally, chemists prepared pyridine or imidazole derivatives to axially coordinate the Fe center of metalloporphyrins. Such coordination stabilized the low-spin state of the center metal configuration to imitate the natural enzyme structure.[2] The axial ligands, including chloride, cyanide and nitrate, were usually coordinated to hemin on both axial sites.[3] However, in natural enzymes, the thiolate ligand dominated the fifth coordination position of metal center of hemin, while the sixth position remained open.[4] Therefore, the determination of single or dual axial interaction between the metal center of metalloporphyrin and the ligand is a challenging endeavor, which usually requires complicated chemical modifications of the metalloporphyrin to control the single-sided coordination.[5]

To address the problem, a four-stranded nucleic acid structure, G-quadruplex (G4), was introduced to bind tightly with hemin to form specific hemin-binding tertiary structure via intramolecular guanine quadraplexes.[6] The resulting G4/hemin complex provided one unoccupied axial site on the center Fe in hemin due to the end-stacking at the terminals of G-quadruplexes against the other positions.[7] In addition, the majority of the hemin in the G4/hemin complex was monomeric, which resulted in a more reactive activation, compared to the aggregated hemin in aqueous solution.[8] The above advantages could bring new opportunities to decode the mechanism on hemin-based axial interaction. Moreover, the application of the single-sided axial coordination of G4/hemin complex as a molecular switch provided great potential in biosensing and intracellular function analysis.

Due to the significance of axial Fe–NO interactions on the biologically relevant process of ferriporphyrin,[9] nitric oxide (NO) was taken as a model for competitive binding of the G4/hemin system. Although hemin-functionalized graphene field-effect transistors showed highly selective electrical detection of NO in physiological conditions,[10a] fluorescent probes were more applicable for NO imaging in living cells.[10b,c] Here, taking advantages of G4/hemin, we present a "signal on" strategy based on fluorescent ligands conjugated G4/hemin complex as signal transduction platform for intracellular NO imaging through competitive axial coordination. To achieve this, a series of fluorescent ligands were first designed by conjugating fluorescein or coumarin fluorophore with amino-containing pyridine/imidazole derivatives. These ligands could selectively interact with G4/hemin via axial coordination, and their fluorescence was quenched due to electron transfer from the fluorophore to transition metals with partially filled d-shells.[11] In the presence of NO target, the coumarin-imidazole ligand was replaced and the fluorescence was recovered for signal readout (Scheme 1 A). In contrast, the fluorescence recovery was infeasible in the free hemin system due to the formation of a six-coordinated Fe–NO hemin complex (Scheme 1 B). Furthermore, after conjugating with gold nanoparticles (AuNPs), the

[a] Dr. L. Zhang,[+] Dr. J. Zhou,[+] F. J. Ma,[+] Prof. H. X. Ju, Prof. J. P. Lei
State Key Laboratory of Analytical Chemistry for Life Science
School of Chemistry and Chemical Engineering
Nanjing University, Nanjing 210023 (P.R. China)
E-mail: hxju@nju.edu.cn
jpl@nju.edu.cn

[b] Dr. L. Zhang,[+] Prof. H. Xu
School of Chemistry and Molecular Engineering, Institute of Advanced Synthesis, Jiangsu National Synergetic Innovation Center for Advanced Materials, Nanjing Tech University, Nanjing 211816 (P.R. China)
E-mail: ias_hxu@njtech.edu.cn

[c] Dr. Q. B. Wang
Laboratory of Immunology for Environment and Health
Shandong Analysis and Test Center, Shandong Academy of Sciences
Jinan 250014 (P.R. China)

[+] These authors contributed equally to this work.

Supporting information and the ORCID identification number(s) for the author(s) of this article can be found under: https://doi.org/10.1002/chem.201804897.

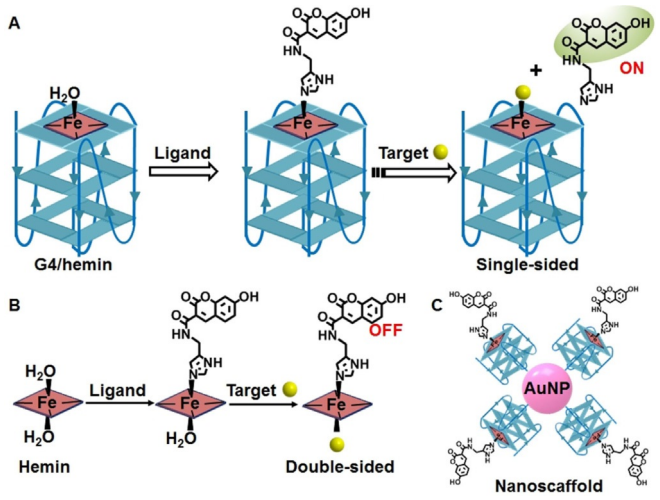

Scheme 1. Schematic illustration of competitive axial coordination of (A) G-quadruplex/hemin and (B) hemin with fluorescent ligand and target, and (C) the structure of **AuNP@G4/hemin-CFI** nanoscaffold.

AuNP@G4-hemin nanoscaffold could specifically recognize and image intracellular NO via competitive axial coordination (Scheme 1C). The relationship between NO and p53 protein activity was explored in living cells by the proposed protocol, showing its broad applications in vivo.

The G4/hemin complex was prepared by incubating a parallel G-quadruplex with hemin for 15 min and characterized with circular dichroism spectra (Figure S1).[12] To investigate the axial coordination effect of G4/hemin complex, five different ligands were firstly synthesized by conjugating fluorescein or coumarin fluorophore with amino-contained pyridine/imidazole derivatives (Figure 1A and S2). As shown in Figure 1B, low fluorescence quenching was observed from the interaction of G4/hemin complex with fluorescein derivatives (ligands **1**–**3**) due to the limitation of steric hindrance effect of the fluorophore containing highly delocalized conjugated structure. However, the axial interaction of coumarin fluorophore-based ligand with G4/hemin slightly increased the fluorescence quenching (ligand **4**). Based on the higher coordination ability of imidazole group than pyridine group,[13] the significant quenching effect was observed after the interaction of G4/hemin with ligand **5** (named as **CFI**) containing coumarin fluorophore and imidazole group (Figure 1B). The formation of a desirable **hemin-CFI** complex was directly confirmed by mass spectrometry with the mass peaks at *m/z* 650.0 and 894.0 (Figure S3).

UV/Vis absorption showed that the free hemin has a Soret absorption band of dimeric absorption centered at 386 nm in aqueous solution (Figure 2A).[14] After incubation with G-quadruplex, a sharp hyperchromicity of the absorption center shifts to about 404 nm represented monomeric hemin, suggesting more reactive hemin in the G4/hemin complex.[15] Interestingly, in the presence of ligand **CFI**, a much more quenched fluorescent intensity of **CFI** was obtained after binding to G4-complexed hemin than free hemin (Figure 2B and Figure S4 in the Supporting Information). Through the UV/Vis spectrometric titration, a higher Log *K* value for binding constant was observed for the G4/hemin complex (Log $K = 4.4$) than free hemin (Log $K = 3.2$) (Figure 2C), mainly due to the high reactivity on the monomeric hemin in G4/hemin complex. From the above investigations, we proposed that G4/hemin complex provided high-reactive axial sites at Fe center of hemin.

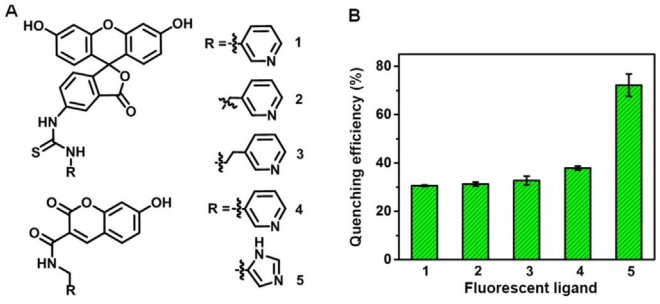

Figure 1. (A) Structures of fluorescent ligands **1**–**5**. (B) Fluorescence quenching efficiency of the corresponding ligands (10 μM) after the axial interactions with G4/hemin complex (10 μM) in 10 mM Tris-HCl buffer (pH 7.4).

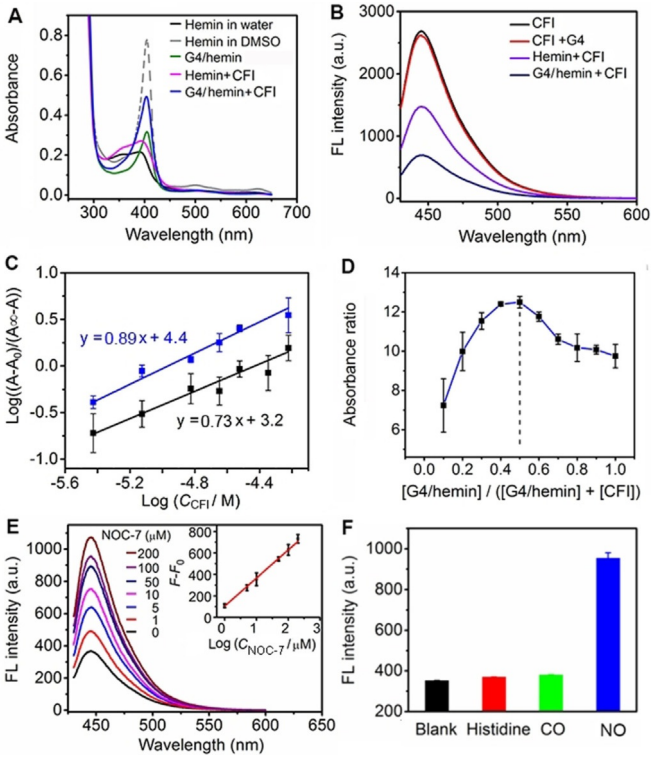

Figure 2. (A) UV/Vis spectra of hemin (7.5 μM) and G4/hemin (7.5 μM equivalent hemin) before and after axial interactions with **CFI** (15 μM) in Tris-HCl, and hemin (7.5 μM) in dimethylsulfoxide (DMSO). (B) Fluorescence spectra of **CFI** (20 μM) in the absence and presence of individual G-quadruplex (10 μM), hemin (20 μM), and G4/hemin complex (20 μM equivalent hemin) in Tris-HCl. $\lambda_{ex} = 397$ nm. (C) Plots of log $[(A-A_0)/(A_\infty-A)]$ vs. Log *C* for UV/Vis spectral change upon titration of **CFI** to hemin (black) and G4/hemin (blue) in Tris-HCl. (D) Job's plot for the binding of **CFI** to G4/hemin complex. The total concentration of hemin and **CFI** was kept constant at 100 μM in Tris-HCl. A_{404}/A_{504} is the ratio of absorbance intensity at 404 to 504 nm of G4/hemin complex. (E) Fluorescence spectral response of **G4/hemin-CFI** (10 μM equivalent hemin) to NOC-7 at marked concentrations. Inset: Plot of $F-F_0$ vs. logarithm value of NOC-7 concentration. (F) Fluorescence response of **G4/hemin-CFI** (blank, 10 μM equivalent hemin) at 445 nm to histidine (200 μM), CORM-3 (a CO donor, 200 μM) and NOC-7 (100 μM) in Tris-HCl.

Upon the assembly of the fluorescent ligand, the obtained **G4/hemin-CFI** caused a mild redshifted Soret absorption band and clearly increased absorbance in the UV/Vis spectrum (Figure 2A).

According to the absorbance ratio change in UV/Vis spectra, Job's plot analysis revealed a 1:1 binding stoichiometry of the coordination reaction (Figure 2D), suggesting a single axial coordination for the Fe center in the G4/hemin complex. The deviation between 0.4–1.0 was mainly attributed to the competitive interaction of the uncomplexed hemin with **CFI**.[16,17] This result can be explained because hemin in G4 has two axial sites, one of which gave way to the interaction within the G-quadruplex structure due to the end-stacking of hemin,[18] leading to one accessible axial site for the additional ligand. The single-sided axial coordination of G4/hemin complex provides a unique competitive platform for biosensing.

After exposure of the **G4/hemin-CFI** complex to a solution of NOC-7 (a common NO donor) or NO solution (Figure S5 and S6), the fluorescence intensity increased dramatically upon addition of NOC-7 in a concentration-dependent manner (Figure 2E). Remarkably, a good linear relationship was observed between the fluorescence enhancement (F_0 and F is the fluorescence intensity in absence and presence of NOC-7, respectively) and the NOC-7 concentration (inset in Figure 2E). After titration of G4/hemin solution with different concentrations of NOC-7 (Figure S7),[19] the binding constant (K_{NO}) was determined by the absorbance change at 404 nm of the G4/hemin spectra, which was about three orders of magnitude larger than that with **CFI**. In addition, the fluorescence quenching of **CFI** by the G4/hemin complex was greatly inhibited when NO had been preferentially coordinated with the metal center. The recovered fluorescence intensity was comparable to the uncomplexed **CFI** (Figure S8), demonstrating the feasibility of competitive axial coordination-based detection mechanism of **G4/hemin-CFI** system.

The structure of **G4/hemin-NO** complex was investigated after the axial replacement reaction (Figure S9). X-ray photoelectron spectroscopy demonstrated that Fe^{II} played the main role in the complex (Figure S9A).[20] As shown in Figure S9B, the electron spin resonance spectrum of the **G4/hemin-NO** complex exhibited the five-coordinate characteristic with a low-spin configuration.[21] In resonance Raman spectrum, the stretching frequency around 718 and 1045 cm^{-1} was assigned to Fe–NO stretching frequency, whereas the N–O stretching mode corresponded to the frequency at 1436 and 1652 cm^{-1} (Figure S9C).[21a] These results successfully identified the formation of **G4/hemin-NO** complex.

Under the same conditions, the **G4/hemin-CFI** complex displayed negligible fluorescence changes in the presence of other species with Fe-coordinated capability including CO and imidazole compound (Figure 2F). Meanwhile, the **hemin-CFI** complex in the absence of G4 showed less than 10% fluorescence recovery in response to NO (Figure S10). We attributed the appearance of weak fluorescence recovery to the following reasons: one is the preferential formation of a six-coordinate NO complex that blocked the signal switch of the replacement of **CFI** by NO;[22] the other is that the hemin aggregates in aqueous solution are less axially reactive with NO than the monomeric hemin in G4/hemin complex, which also reduced the sensitivity.[21a]

For efficient imaging of NO in living cells, a typical 13 nm Au nanoparticle (characterized in Figure S11) was employed as the highly efficient nanocarrier for enhancing the local concentration in cells,[23] as well as preserving the G4 DNA sequence from the effect of intracellular DNA enzymes (Figure S12). The nanoscaffold (**AuNP@G4/hemin-CFI**) was prepared by the conjugation AuNP with **G4/hemin-CFI** and folate-functionalized polyethylene glycol via Au–S bond, and was characterized by the fluorescence and UV/Vis spectra (Figure S13). The corresponding number of G4 DNA on each Au nanoparticle was calculated to be 92 from the absorbance at 260 nm.

To verify the feasibility of the nanoscaffold to NO, the concentration-dependent fluorescence increase was shown in vitro (Figure 3A). The nanoscaffold possessed good biocompatibility as cells treated with the probe for 4 h exhibited an acceptable viability of ≈91% (Figure S14). After the folate receptor-targeted endocytosis (Figure S15), the probe could be delivered into lysosome (Figure S16). The fluorescence of the nanoscaffold was clearly enhanced in response to NOC-7 transfected cell for 15 min (Figure S17). Meanwhile, the confocal fluorescence images of the NOC-7 treated cells showed bright fluorescence (Figure 3B), which displayed more lighted fluorescence in the conditions of pre-treated with cytokine stimulant.[24] The measurements of fluorescence intensity from the correspondingly extracted cell agreed with the results from the confocal fluo-

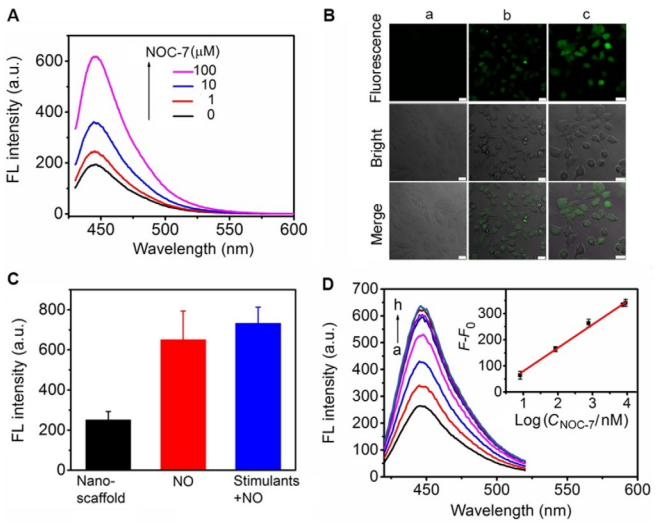

Figure 3. (A) Fluorescence spectral response of the **AuNP@G4/hemin-CFI** nanoscaffold (10 μM equivalent hemin) to NOC-7 solution at marked concentrations. (B) Confocal fluorescence images and (C) fluorescence measurements on multimode microplate reader of HeLa cells incubated with the nanoscaffold (a, 0.1 mM equivalent hemin), the mixture of NOC-7 (20 μM) and the nanoscaffold before (b) and after (c) pre-treated with NO stimulants (cytokines, a combination of 50 ng mL^{-1} TNF-α and 25 ng mL^{-1} IFN-γ). Scale bars: 25 μm. (D) Fluorescence spectral response of the nanoscaffold (0.1 mM equivalent hemin) to transfected NOC-7 in living cells at the concentration of 0, 8.0 nM, 86 nM, 770 nM, 7.4 μM, 9.0 μM, 10.8 μM, and 18.8 μM (from a to h). Inset: Plot of $F-F_0$ vs. logarithm value of NOC-7 concentration. F_0 and F are the fluorescence intensity in the absence and presence of NOC-7, respectively.

rescence images (Figure 3C), suggesting the specific response of intracellular NO.[25] Moreover, maintaining the fluorescence of the above treated HeLa cells under low temperatures excluded down-stream effects of NO signaling and changes in cellular properties (Figure S18).[26] The plot of cellular fluorescence intensity versus the amount of NOC-7 transfected into the cell showed a good linear relationship with a related coefficient of 0.995 in a wide range of concentrations (Figure 3D). Thus, the designed **AuNP@G4/hemin-CFI** nanoscaffold could be used for in situ imaging and detection of intracellular NO.

Finally, we applied the nanoscaffold to investigate the quantitative relationship of the NO and p53 protein.[27] HeLa cells were first incubated with different amounts of cytokines for 48 h, and then treated with the nanoscaffold for 4 h. After washing with PBS three times, these cells were conducted on multimode microplate reader for fluorescence measurements in Figure 4A. Meanwhile, the resulted cell extract pre-treated as above was detected via in vitro nitric oxide assay kit (Figure 4B) and p53 colorimetric kit (Figure 4C) individually to get the absorbance at 540 and 450 nm generated from the specific reaction in the kits, respectively. The corresponding NO concentration and p53 activation could be calculated by using linear relationship of absorbance vs. logarithmic value of their standard concentration in the kit accordingly. Combining with the above analyses, a plot of p53 activation versus logarithmic value of intracellular inducible NO concentration in HeLa cell was obtained and followed a linear regression equation of C_{p53} (ng μL^{-1}) = 0.078 × Log C_{NO} (nM) − 0.037 (Figure 4D), which indicated that the designed nanoscaffold could be used for analysis of intracellular p53-mediated physiological process. Therefore, a fluorescent imaging method was achieved for chemical analysis of biomolecular interaction using the designed competitive axial coordination system.

In conclusion, we delicately constructed the single-sided axial coordination system of G4/hemin complex as a molecular switch instead of using the common catalytic property of G4/hemin. The G4/hemin demonstrated more powerful potential in aqueous axial ligation compared to the uncomplexed hemin. The main reasons are as follows: Firstly, G4/hemin has more reactive monomeric hemin, which inhibits aggregation in aqueous solution; secondly, the single unoccupied axial site at the Fe center of G4/hemin enhances the binding capacity of the axial ligands. Therefore, the unique sensing strategy of **G4/hemin-CFI** was established for NO detection via single-sided competitive axial coordination, which was infeasible in the free hemin system due to the formation of a six-coordinated Fe–NO hemin complex. Furthermore, the conjugated **AuNP@G4/hemin-CFI** nanoscaffold not only realized in situ imaging and detection of intracellular NO, but also was successfully used to quantify the level of the p53 protein activity in the NO-related biological process, providing a new opportunity to understand the complicated physiological pathway of NO.

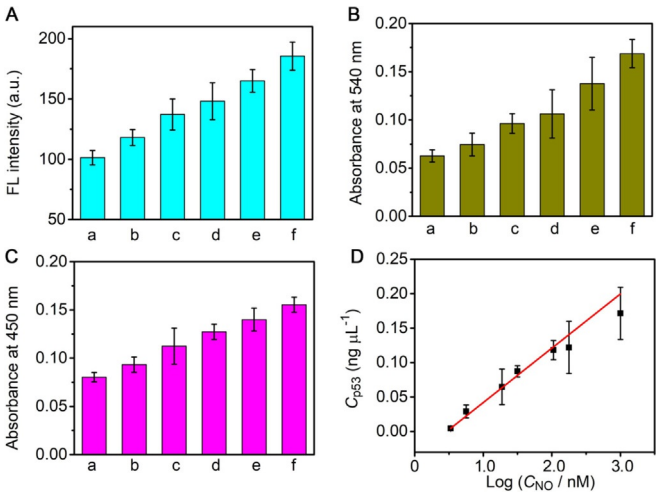

Figure 4. (A) Fluorescence intensities of HeLa cells stimulated with different concentrations of cytokines for 48 h and then the nanoscaffold (0.1 mM equivalent hemin) for 4 h. Cytokine, a combination of TNF-α and IFN-γ with the concentrations of 5/2.5, 10/5, 20/10, 30/15, 40/20, and 50/25 ng mL^{-1} from a to f. (B) UV/Vis absorbance at 540 nm using nitric oxide colorimetric assay kit for extracts of HeLa cells treated as in (A). (C) UV/Vis absorbance at 450 nm using p53 kit for extracts of HeLa cells treated as in (A). (D) Plot of p53 activity vs. logarithmic value of the intracellular inducible NO concentration in HeLa cells incubated with the nanoscaffold (0.1 mM equivalent hemin).

Acknowledgements

We gratefully acknowledge the National Natural Science Foundation of China (21675084, 21605082, 21635005) and Natural Science Foundation of Jiangsu Province (BK20160641).

Conflict of interest

The authors declare no conflict of interest.

Keywords: axial coordination · biosensors · fluorescent probes · G-quadruplex-hemin · imaging

[1] J. A. McIntosh, T. Heel, A. R. Buller, L. Chio, F. H. Arnold, *J. Am. Chem. Soc.* **2015**, *137*, 13861 – 13865.
[2] a) R. L. Khade, Y. W. Yang, Y. L. Shi, Y. Zhang, *Angew. Chem. Int. Ed.* **2016**, *55*, 15058 – 15061; *Angew. Chem.* **2016**, *128*, 15282 – 15285; b) P. K. Das, S. Samanta, A. B. McQuarters, N. Lehnert, A. Dey, *Proc. Natl. Acad. Sci. USA* **2016**, *113*, 6611 – 6616; c) W. Auwärter, D. Écija, F. Klappenberger, J. V. Barth, *Nat. Chem.* **2015**, *7*, 105 – 120.
[3] a) R. Kumar, H. Matsumura, S. Lovell, H. Yao, J. C. Rodríguez, K. P. Battaile, P. Moënne-Loccoz, M. Rivera, *Biochemistry* **2014**, *53*, 2112 – 2125; b) N. V. Shokhirev, F. A. Walker, *J. Biol. Inorg. Chem.* **1998**, *3*, 581 – 594.
[4] W. R. Scheidt, J. F. Li, J. T. Sage, *Chem. Rev.* **2017**, *117*, 12532 – 12563.
[5] S. K. Sharma, A. W. Schaefer, H. Lim, H. Matsumura, P. Moënne-Loccoz, B. Hedman, K. O. Hodgson, E. I. Solomon, K. D. Karlin, *J. Am. Chem. Soc.* **2017**, *139*, 17421 – 17430.
[6] a) P. Travascio, Y. F. Li, D. Sen, *Chem. Biol.* **1998**, *5*, 505 – 517; b) S. Burge, G. N. Parkinson, P. Hazel, A. K. Todd, S. Neidle, *Nucleic Acids Res.* **2006**, *34*, 5402 – 5415; c) E. Golub, R. Freeman, I. Willner, *Angew. Chem. Int. Ed.* **2011**, *50*, 11710 – 11714; *Angew. Chem.* **2011**, *123*, 11914 – 11918; d) S. Wang, L. Yue, Z. Y. Li, J. J. Zhang, H. Tian, I. Willner, *Angew. Chem. Int. Ed.* **2018**, *57*, 8105 – 8109; *Angew. Chem.* **2018**, *130*, 8237 – 8241.
[7] a) X. J. Yang, C. L. Fang, H. C. Mei, T. J. Chang, Z. H. Cao, D. H. Shangguan, *Chem. Eur. J.* **2011**, *17*, 14475 – 14484; b) M. Wang, Z, Mao, T. S. Kang, C. Y. Wong, J. L. Mergny, C. H. Leung, D. L. Ma, *Chem. Sci.* **2016**, *7*, 2516 – 2523; c) Y. Yamamoto, M. Kinoshita, Y. Y. Katahira, H. Shimizu, Y. Di, T. Shibata, H. L. Tai, A. Suzuki, S. Neya, *Biochemistry* **2015**, *54*, 7168 –

7177; d) K. Saito, H. Tai, M. Fukaya, T. Shibata, R. Nishimura, S. Neya, Y. Yamamoto, *J. Biol. Inorg. Chem.* **2012**, *17*, 437 – 445.

[8] a) Y. H. Guo, J. L. Chen, M. P. Cheng, D. Monchaud, J. Zhou, H. X. Ju, *Angew. Chem. Int. Ed.* **2017**, *56*, 16636 – 16640; *Angew. Chem.* **2017**, *129*, 16863 – 16867; b) H. Xu, Q. Li, L. H. Wang, Y. He, J. Y. Shi, B. Tang, C. H. Fan, *Chem. Soc. Rev.* **2014**, *43*, 2650 – 2661; c) J. Zheng, R. H. Yang, M. L. Shi, C. C. Wu, X. H. Fang, Y. H. Li, J. S. Li, W. H. Tan, *Chem. Soc. Rev.* **2015**, *44*, 3036 – 3055; d) E. Golub, H. B. Albada, W. C. Liao, Y. Biniuri, I. Willner, *J. Am. Chem. Soc.* **2016**, *138*, 164 – 172.

[9] a) E. Eroglu, B. Gottschalk, S. Charoensin, S. Blass, H. Bischof, R. Rost, C. T. Madreiter-Sokolowski, B. Pelzmann, E. Bernhart, W. Sattler, S. Hallström, T. Malinski, M. Waldeck-Weiermair, W. F. Graier, R. Malli, *Nat. Commun.* **2016**, *7*, 10623; b) M. Sato, N. Hida, Y, Umezawa, *Proc. Natl. Acad. Sci. USA* **2005**, *102*, 14515 – 14520.

[10] a) S. Jiang, R. Cheng, X. Wang, T. Xue, Y. Liu, A. Nel, Y. Huang, X. F. Duan, *Nat. Commun.* **2013**, *4*, 2225; b) E. Sasaki, H. Kojima, H. Nishimatsu, Y. Urano, K. Kikuchi, Y. Hirata, T. Nagano, *J. Am. Chem. Soc.* **2005**, *127*, 3684 – 3685; c) Y. Gabe, Y. Urano, K. Kikuchi, H. Kojima, T. Nagano, *J. Am. Chem. Soc.* **2004**, *126*, 3357 – 3367.

[11] S. A. Hilderbrand, M. H. Lim, S. J. Lippard, *J. Am. Chem. Soc.* **2004**, *126*, 4972 – 4978.

[12] J. Kypr, I. Kejnovska, D. Renciuk, M. Vorlickova, *Nucleic Acids Res.* **2009**, *37*, 1713 – 1725.

[13] J. Chlistunoff, J. M. Sansiñena, *J. Phys. Chem. C* **2014**, *118*, 19139 – 19149.

[14] T. Xue, S. Jiang, Y. Q. Qu, Q. Su, R. Cheng, S. Dubin, C. Y. Chiu, R. Kaner, Y. Huang, X. F. Duan, *Angew. Chem. Int. Ed.* **2012**, *51*, 3822 – 3825; *Angew. Chem.* **2012**, *124*, 3888 – 3891.

[15] T. Li, L. L. Shi, E. K. Wang, S. J. Dong, *Chem. Eur. J.* **2009**, *15*, 1036 – 1042.

[16] a) Y. Zhao, P. E. Brandish, D. P. Ballou, M. A. Marletta, *Proc. Natl. Acad. Sci. USA* **1999**, *96*, 14753 – 14758; b) E. Martin, V. Berka, I. Sharina, A. L. Tsai, *Biochemistry* **2012**, *51*, 2737 – 2746.

[17] C. M. Coyle, K. M. Vogel, T. S. Rush, P. M. Kozlowski, R. Williams, T. G. Spiro, Y. Dou, M. Ikeda-Saito, J. S. Olson, M. Z. Zgierski, *Biochemistry* **2003**, *42*, 4896 – 4903.

[18] T. J. Chang, H. M. Gong, P. Ding, X. J. Liu, W. G. Li, T. Bing, Z. H. Cao, D. H. Shangguan, *Chem. Eur. J.* **2016**, *22*, 4015 – 4021.

[19] Z. C. Chen, L. H. Wang, J. P. M. Schelvis, *Biochemistry* **2003**, *42*, 2542 – 2551.

[20] C. Ruby, B. Humbert, J. Fusy, *Surf. Interface Anal.* **2000**, *29*, 377 – 380.

[21] a) A. P. Hunt, N. Lehnert, *Acc. Chem. Res.* **2015**, *48*, 2117 – 2125; b) J. Igarashi, A. Sato, T. Kitagawa, T. Yoshimura, S. Yamauchi, I. Sagami, T. Shimizu, *J. Biol. Chem.* **2004**, *279*, 15752 – 15762.

[22] J. F. Li, Q. Peng, A. G. Oliver, E. E. Alp, M. Y. Hu, J. Y. Zhao, J. T. Sage, W. R. Scheidt, *J. Am. Chem. Soc.* **2014**, *136*, 18100 – 18110.

[23] a) X. A. Wu, C. H. J. Choi, C. Zhang, L. L. Hao, C. A. Mirkin, *J. Am. Chem. Soc.* **2014**, *136*, 7726 – 7733; b) X. P. Xie, J. F. Liao, X. R. Shao, Q. S. Li, Y. F. Lin, *Sci. Rep.* **2017**, *7*, 3827.

[24] N. M. Druzhyna, S. I. Musiyenko, G. L. Wilson, S. P. LeDoux, *J. Biol. Chem.* **2005**, *280*, 21673 – 21679.

[25] C. J. Reinhardt, E. Y. Zhou, M. D. Jorgensen, G. Partipilo, J. Chan, *J. Am. Chem. Soc.* **2018**, *140*, 1011 – 1018.

[26] R. A. Dulce, V. Mayo, E. B. Rangel, W. Balkan, J. M. Hare, *Circ. Res.* **2015**, *116*, 46 – 55.

[27] L. J. Hofseth, S. Saito, S. P. Hussain, M. G. Espey, K. M. Miranda, Y. Araki, C. Jhappan, Y. Higashimoto, P. J. He, S. P. Linke, M. M. Quezado, I. Zurer, V. Rotter, D. A. Wink, E. Appella, C. C. Harris, *Proc. Natl. Acad. Sci. USA* **2003**, *100*, 143 – 148.

Manuscript received: September 26, 2018
Revised manuscript received: November 3, 2018
Accepted manuscript online: November 8, 2018
Version of record online: December 11, 2018